Supporting Information

Ligand-based modulation of the electronic structure at metal nodes in MOF to promote oxygen evolution reaction

Wang Hao, Mingzheng Gu, Xiaomin Huang, An Gao, Xudong Liu, Ping Sun, and Xiaojun Zhang*

Key Laboratory of Chem-Biosensing, Key Laboratory of Functional Molecular Solids, College of Chemistry and Materials Science, Anhui Normal University, Wuhu 241000, P. R. China.

*E-mail for Xiaojun Zhang: xjzhang@ahnu.edu.cn

1. Experimental Procedures

Materials.

Imidazole, 2-Methylimidazole(2-mIm), 2-Nitroimidazole(2-nIm), Imidazole-2-carboxaldehyde(2-Ica), Cobalt acetate tetrahydrate（$Co(OAC)_2·4H_2O$）, Zinc acetate dihydrate（$Zn(OAC)_2·2H_2O$）, Nickel acetate tetrahydrate（$Ni(OAC)_2·4H_2O$）, high-purity deionized water (DI-water, resistance 18 MΩ cm^{-1}). N,N-dimethylformamide (DMF), methanol (CH_3OH), Ethanol (C_2H_5OH), Potassium Hydroxide (KOH). All reagents purchased from Aladdin Ltd. (Shanghai, China) were used as received without further purification.

Pretreatment of copper foam (CF):

The copper foam was cut into a size of 2*4 cm^2, and the surface oxide layer was removed by ultrasonic washing with dilute hydrochloric acid, the surface organic matter was removed by ultrasonic washing with acetone, respectively. Then, deionized water and anhydrous ethanol were ultrasonically washed for several times for reserve.

Synthesis of ZIF-8.

$Zn[C_6H_6N_4]CH_3$ (ZIF-8) was prepared according to a previously reported procedure with slight modifications. In a typical synthetic procedure, 110 mg of $Zn(OAC)_2·2H_2O$

and 164 mg of 2-Methylimidazole (2-mIm) were first added to 5 mL and 10 mL of methanol, respectively, with constant stirring until all solid precursors were completely dissolved to obtain solutions A and B. The resulting solution A was poured into solution B and stirred for 2.5 h at room temperature. After the reaction was completed, the solid MOFs were collected by high-speed centrifugation at 6500 rpm and washed thoroughly with methanol three times. Finally, it was dried for 12 hours under 60℃ conditions under vacuum.

ZIF-1 was prepared by a similar method using imidazole instead of 2-mIm.

Synthesis of ZIF-65

ZIF-65 was prepared by a similar method using 2-nIm instead of 2-mIm, and 110 mg of $Zn(OAC)_2 \cdot 2H_2O$ and 226 mg of 2-Nitroimidazole(2-nIm) were added to 5 mL of methanol and 10 mL of DMF, respectively, and other conditions were unchanged.

Synthesis of ZIF-90

First, 110 mg of $Zn(OAC)_2 \cdot 2H_2O$ and 192 mg of Imidazole-2-carboxaldehyde (2-Ica) were added to 5 mL of methanol and 10 mL of DMF, respectively, and stirred continuously until all solid precursors were completely dissolved to obtain solutions A and B. Then, the resulting solution A was poured into solution B and stirred at room temperature for 2.5 h. After the reaction was completed, the solids were collected by high-speed centrifugation at 6500 rpm and washed thoroughly with methanol three times. Finally, it was dried for 12 hours under 60℃ conditions under vacuum.

Synthesis of $Co[C_6H_6N_4]X$

$Co[C_6H_6N_4]CH_3$ (ZIF-67) was synthesized by the following procedure. Firstly, 125 mg of $Co(OAC)_2 \cdot 4H_2O$ and 164 mg of 2-methylimidazole (2-mIm) were added to 5 mL and 10 mL of methanol, respectively, and stirred continuously until all solid precursors were completely dissolved to obtain solutions A and B. Then, the resulting solution A was poured into solution B and stirred at room temperature for 2.5 h. After the reaction was completed, the solids were collected by high-speed centrifugation at 6500 rpm and washed thoroughly with methanol three times. Finally, it was dried for 12 hours under 60℃ conditions under vacuum.

$Co[C_6H_6N_4]H$ was prepared by a similar method using imidazole instead of 2-mIm.

$Co[C_6H_6N_4]NO_2$ was synthesized by the following procedure. First, 125 mg of $Co(OAC)_2{\cdot}4H_2O$ and 226 mg of 2-Nitroimidazole (2-nIm) were added to 10 mL of methanol and 10 mL of DMF, respectively, with other reaction conditions unchanged.

$Co[C_6H_6N_4]CHO$ was synthesized by the following procedure. Firstly, 125 mg of $Co(OAC)_2{\cdot}4H_2O$ and 192 mg of Imidazole-2-carboxaldehyde (2-Ica) were added to 10 mL of methanol and 10 mL of DMF, respectively, and other reaction conditions remained unchanged.

Synthesis of $Ni[C_6H_6N_4]X$

$Ni[C_6H_6N_4]CH_3$ was synthesized by the following procedure. Firstly, 125 mg of $Ni(OAC)_2{\cdot}4H_2O$ and 164 mg of 2-methylimidazole (2-mIm) were added to 10 mL of methanol, respectively, and stirred continuously until all solid precursors were completely dissolved to obtain solutions A and B. Then, the resulting solution A was poured into solution B and stirred at room temperature for 2.5 h. After the reaction was completed, the solids were collected by high-speed centrifugation at 6500 rpm and washed thoroughly with methanol three times. Finally, it was dried for 12 hours under 60℃ conditions under vacuum.

$Ni[C_6H_6N_4]H$ was prepared by a similar method using imidazole instead of 2-mIm.

$Ni[C_6H_6N_4]NO_2$ was synthesized by the following procedure. First,125 mg of $Ni(OAC)_2{\cdot}4H_2O$ and 226 mg of 2-Nitroimidazole (2-nIm) were added to 8 mL of methanol and 10 mL of DMF, respectively, with other reaction conditions unchanged.

$Ni[C_6H_6N_4]CHO$ was synthesized by the following procedure. First, 125 mg of $Ni(OAC)_2{\cdot}4H_2O$ and192 mg of Imidazole-2-carboxaldehyde (2-Ica) were added to 10 mL of methanol and 10 mL of DMF, respectively, and stirred continuously until all solid precursors were completely dissolved to obtain solutions A and B. Then, the resulting solution B was poured into solution A and stirred at room temperature for 2.5 h. After the reaction was completed, the solids were collected by high-speed centrifugation at 6500 rpm and washed thoroughly with methanol three times. Finally, it was dried for 12 hours under 60℃ conditions under vacuum.

Materials Characterization.

X-ray diffraction (XRD) pattern was recorded using a PANalytical X-pert

diffractometer with Cu-Kα radiation. The morphology of the samples was observed by scanning electron microscopy (SEM) and energy-dispersive spectroscopy (EDS, Hitachi S-4800) and transmission electron microscopy (TEM, FEI Tecnai G220). The chemical compositions of the prepared catalysts were examined by X-ray photoelectron spectrometer (Escalab 250Xi, Thermo Fisher).

Electrochemical Measurements.

First, the active material (the synthesized sample), the conductive agent (carbon nanotubes) and the binder (PVDF) were dispersed in C5H9NO (NMP) at a mass ratio of 8:1:1 to make slurry and then applied to the surface of the treated copper foam. Finally, the activated material was dried at 60 ℃ for 12 h in a vacuum drying oven. The as-prepared working electrode has an area of 1 cm^2 with a loading of approximately 0.3~0.5mg cm^2. Cyclic voltammetry (CV), linear sweep voltammetry (LSV), electrochemical impedance spectroscopy (EIS), and chronopotentiometry were performed using a three-electrode electrochemical system. In this system, CF coated with electrocatalyst is directly used as the working electrode. Ag/AgCl (saturated with 4 M KCl) and platinum wire were used as the reference and counter electrodes, respectively. 1.0 M KOH solution was used as electrolyte. The catalysts were first activated by a CVs scan with a scan rate of 5 $mV \cdot S^{-1}$ until reaching a stable state. LSV curves were obtained at a scan rate of 5 $mV \cdot S^{-1}$. Tafel slopes were obtained from the LSV curves by plotting the potential against log (current density). Chronopotentiometry measurements were carried out at a current density of 20 mA cm^{-2} to evaluate the long-term stability of the samples. The EIS was measured using AC impedance spectroscopy over a frequency range of 0.01 Hz-10000 Hz.

2. **Supplementary Figures**

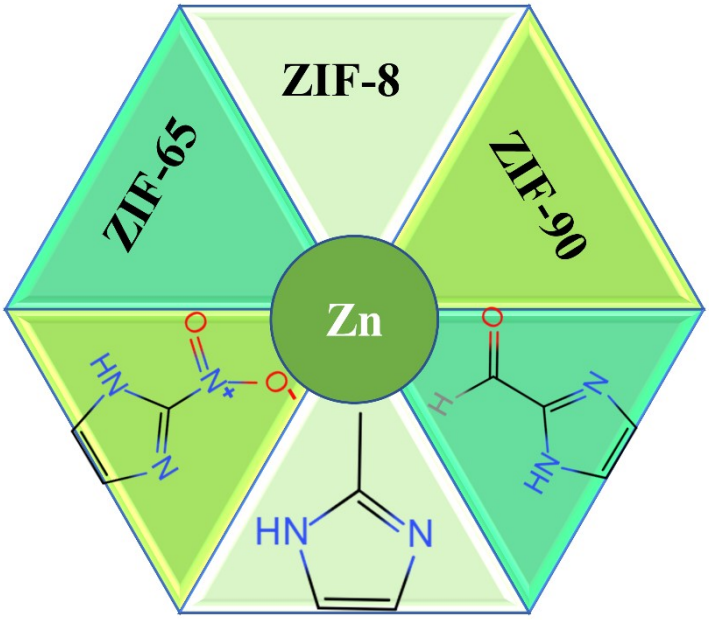

Figure S1. Structural formula of imidazole ligand and MOF synthesis route

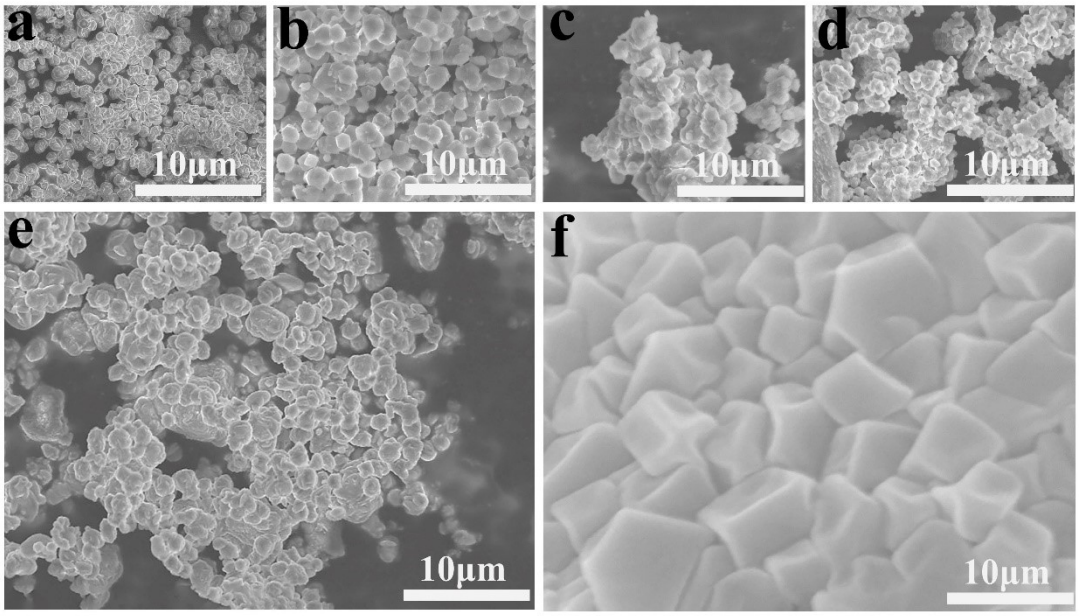

Figure S2. SEM images of reaction time 0.5h(a) and 2.5h(b), solvent water(c) and DMF(d), molar ratio 1:2(e) and 1:6(f) on the morphology of ZIF-8.

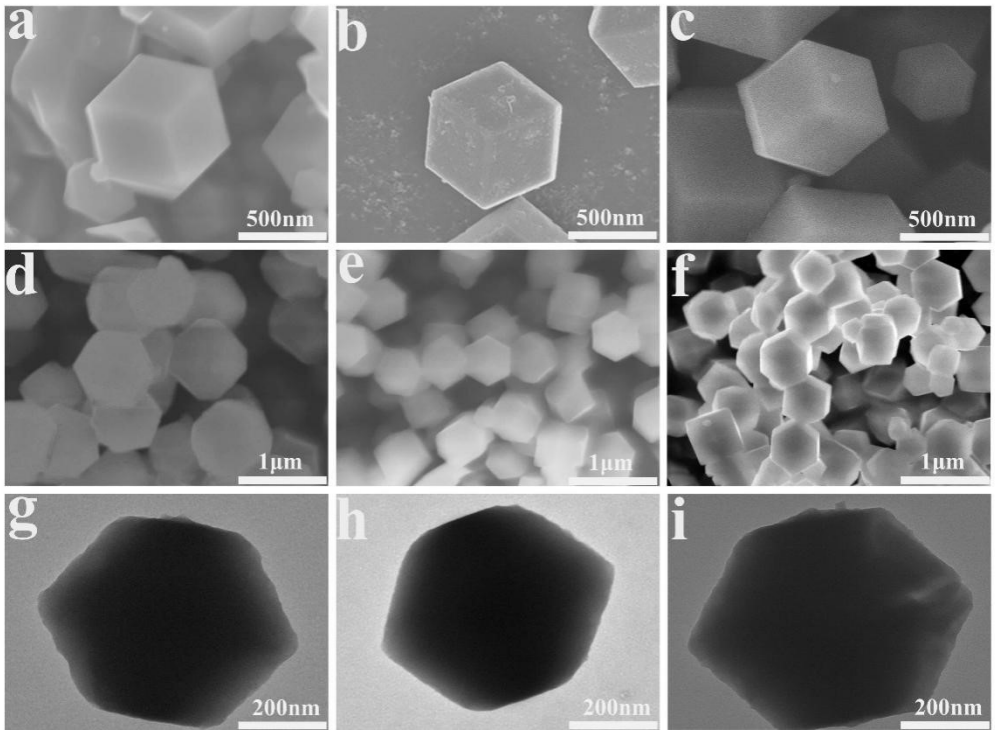

Figure S3. SEM images of ZIF-1(a, d), ZIF-65(b, e), ZIF-90(c, f), TEM images of ZIF-1(g), ZIF-65(h), ZIF-90(i).

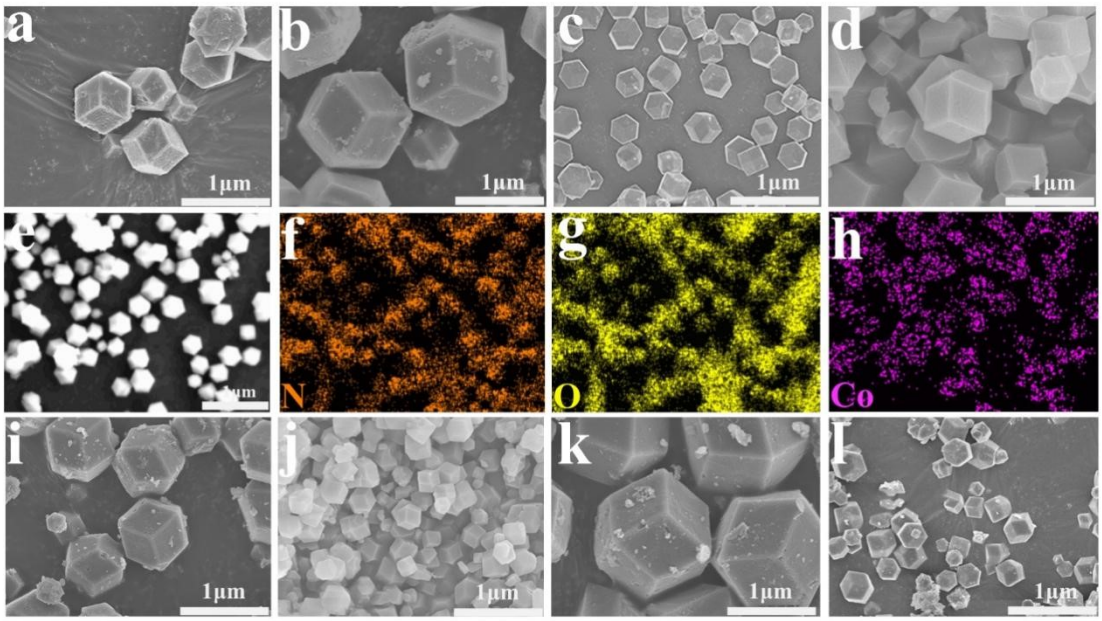

Figure S4. SEM images of $Co[C_6H_6N_4]H$ (a), $Co[C_6H_6N_4]CH_3$(b), $Co[C_6H_6N_4]NO_2$ (c), $Co[C_6H_6N_4]CHO$ (d), e-h) EDX elemental mapping images of N, O and Co elements for the $Co[C_6H_6N_4]NO_2$ sample, SEM images of $Ni[C_6H_6N_4]H$(i), $Ni[C_6H_6N_4]CH_3$(j), Ni $[C_6H_6N_4]NO_2$ (k), Ni $[C_6H_6N_4]CHO$(l).

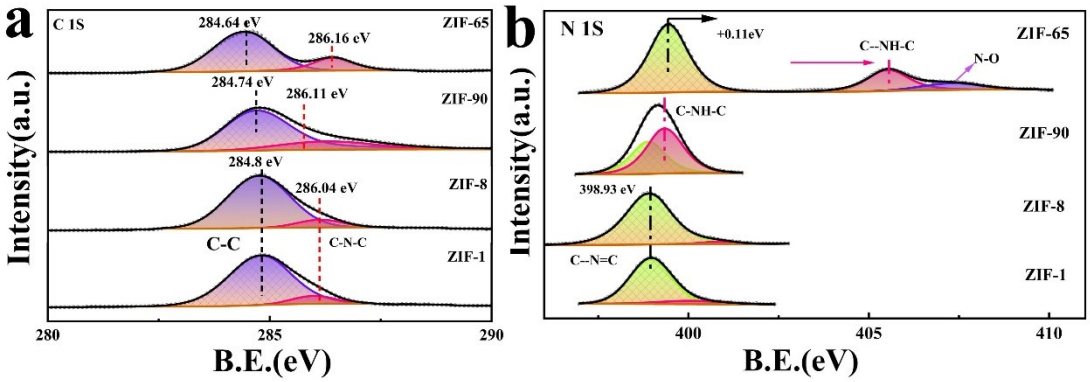

Figure S5. (a) High-resolution XPS spectra of C 1S region survey spectrum of ZIF-1, ZIF-8, ZIF-90 and ZIF-65, (b) N 1s region survey spectrum of ZIF-1, ZIF-8, ZIF-90 and ZIF-65.

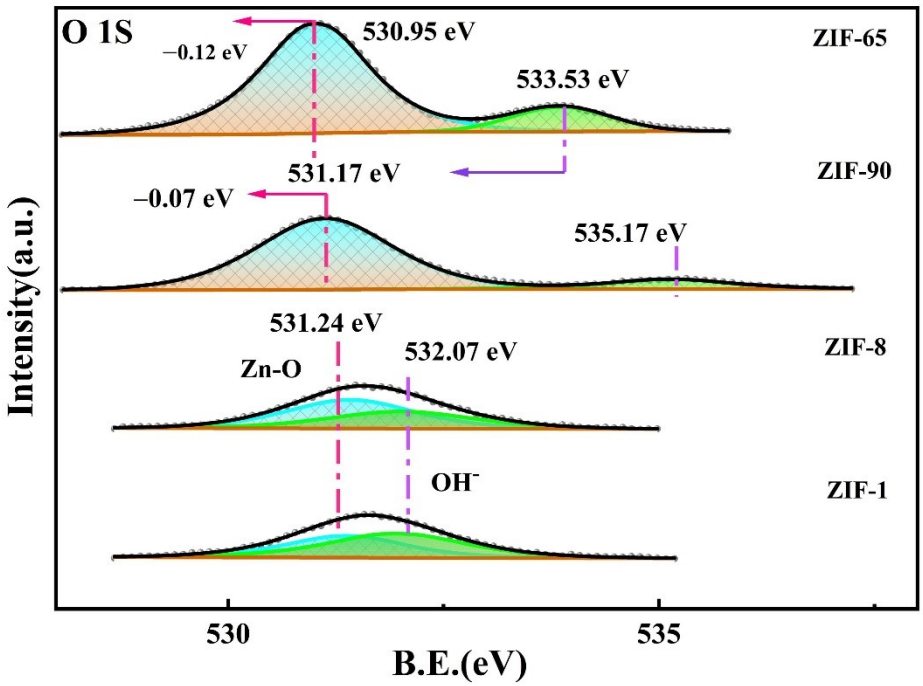

Figure S6. High-resolution XPS spectra of O 1S region survey spectrum of ZIF-1, ZIF-8, ZIF-90 and ZIF-65.

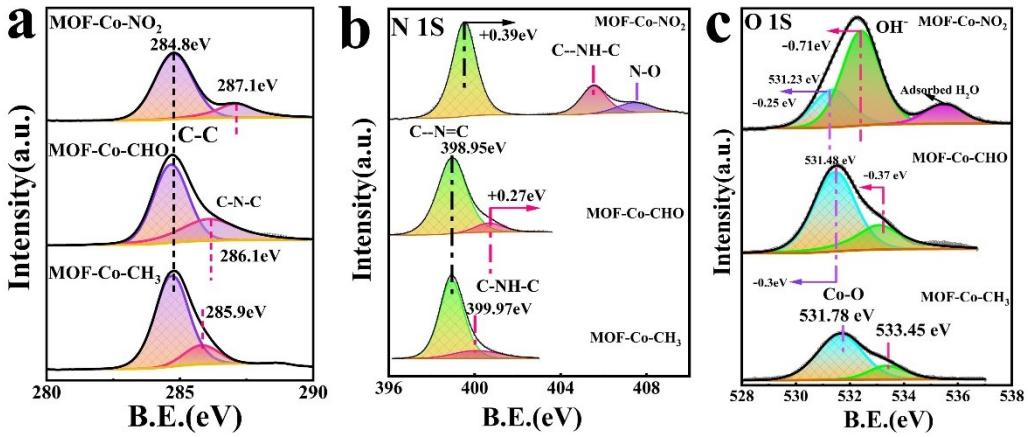

Figure S7. XPS images of C 1S(a), N 1S(b) and O 1S(c) region survey spectrum of $Co[C_6H_6N_4]CH_3$, $Co[C_6H_6N_4]NO_2$ and $Co[C_6H_6N_4]CHO$.

We also analyzed the high-resolution XPS spectra of the C 1S, N 1S and O 1S energy levels in ZIF-1, ZIF-8, ZIF-90 and ZIF-65. The C 1S and O 1S energy levels are negatively shifted to different degrees, as shown in Figures S6 and S7. The ZIF-65 shift is larger (-0.16 eV for C 1S and -0.12 eV for O 1S), while N 1S is positively shifted corresponding to the energy level spectrum of Zn 2P. This suggests that the strong attacking electron group (2-nIm) can properly modulate the electronic structure of Zn center and optimize the adsorption of reaction intermediates, thus improving the electrocatalytic performance.

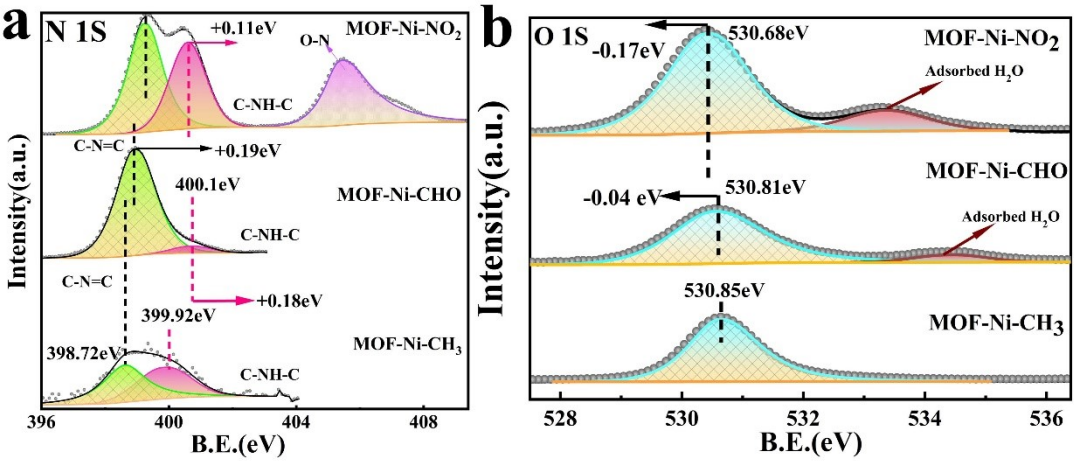

Figure S8. XPS images of C 1S(a) and N 1S(b) region survey spectrum of $Ni[C_6H_6N_4]CH_3$, $Ni\ [C_6H_6N_4]NO_2$ and $Ni\ [C_6H_6N_4]CHO$.

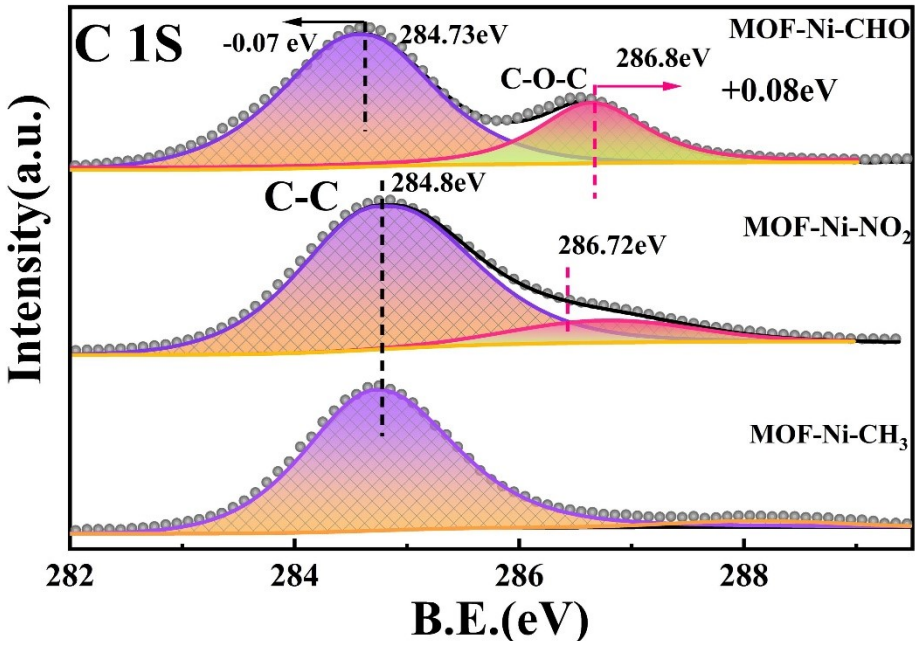

Figure S9. XPS images of C 1S region survey spectrum of Ni[$C_6H_6N_4$]CH_3, Ni [$C_6H_6N_4$]NO_2 and Ni [$C_6H_6N_4$]CHO.

Similarly, high-resolution XPS spectra of the energy levels of C 1S, N 1S and O 1S in Co[$C_6H_6N_4$]X and Ni[$C_6H_6N_4$]X were analyzed, as shown in Figures S7-S9, with different degrees of negative shifts of the C 1S (-0.07 eV) and O 1S (-0.71 eV) energy levels for 2-nIm ligands, respectively, and a positive shift of N 1S (+0.11 eV) corresponding to the metal center corresponds.

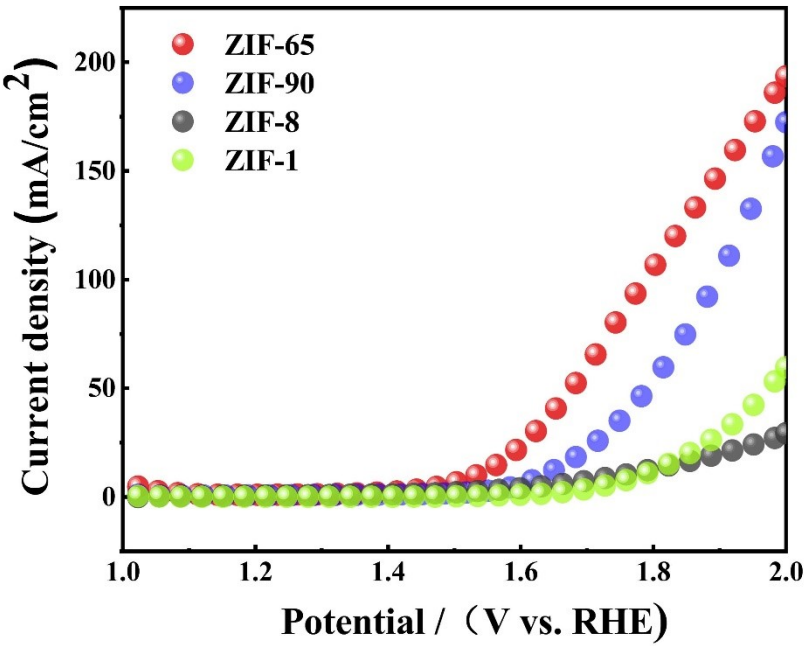

Figure S10. LSV curves of ZIF-1, ZIF-8, ZIF-90 and ZIF-65.

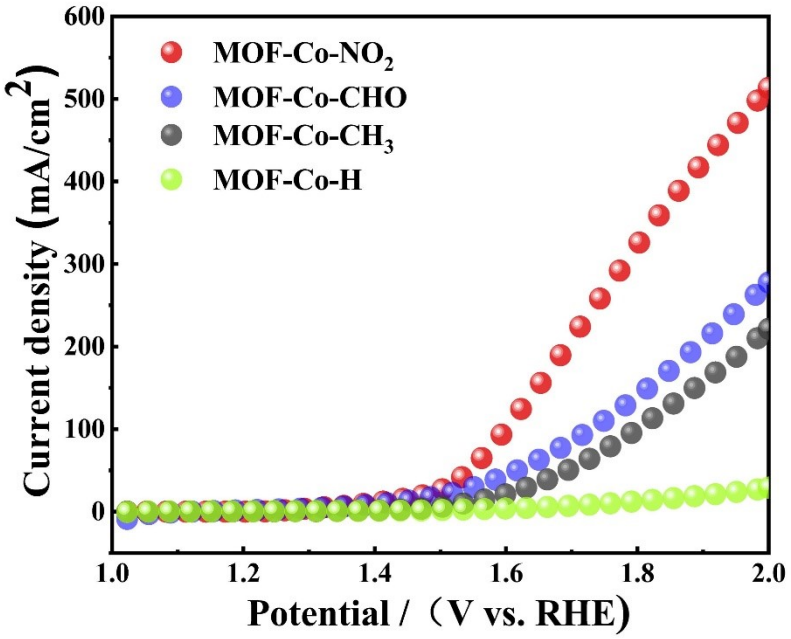

Figure S11. LSV curves of Co $[C_6H_6N_4]H$, $Co[C_6H_6N_4]CH_3$, $Co[C_6H_6N_4]NO_2$ and Co $[C_6H_6N_4]CHO$.

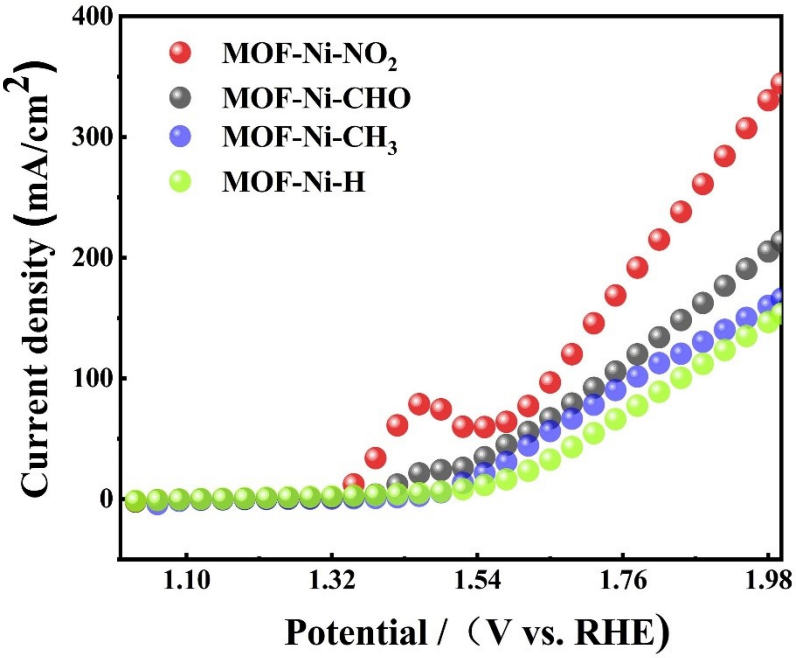

Figure S12. LSV curves of $Ni[C_6H_6N_4]H$, $Ni[C_6H_6N_4]CH_3$, $Ni[C_6H_6N_4]NO_2$ and Ni $[C_6H_6N_4]CHO$.

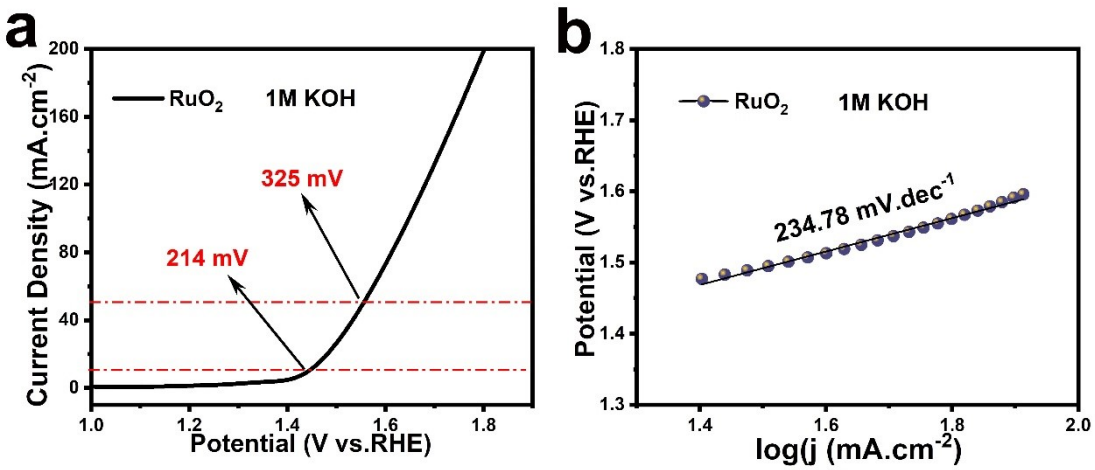

Figure S13. OER performance of RuO_2 in 1.0 M KOH. (a) LSV curves, (b) Tafel plots of OER.

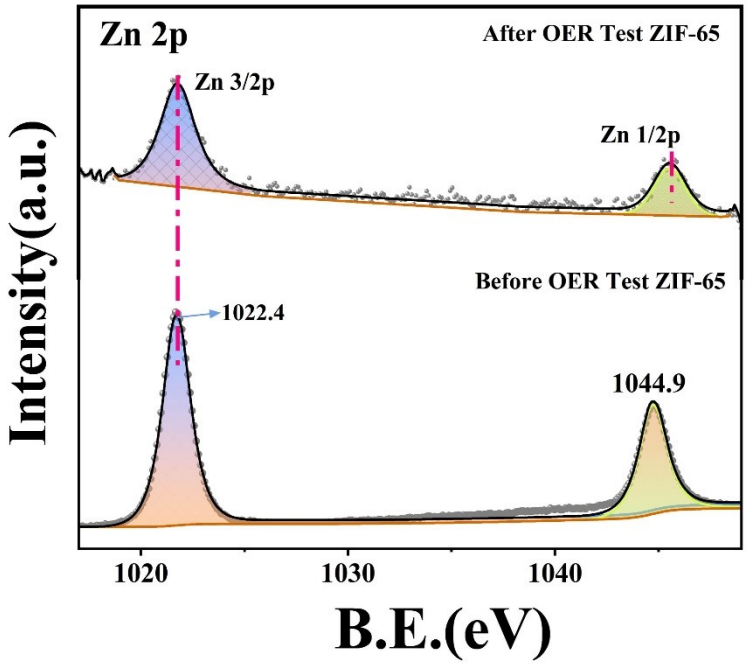

Figure S14. XPS spectra of $Zn[C_6H_6N_4]NO_2$ samples after OER test.

We also analyzed the high-resolution XPS spectra of the individual elemental energy levels before and after the ZIF-65 reaction. As shown in Figure S14, the Zn 2P energy level spectra are not significantly shifted. The stability of Zn 2+ involved in the reaction

is good.

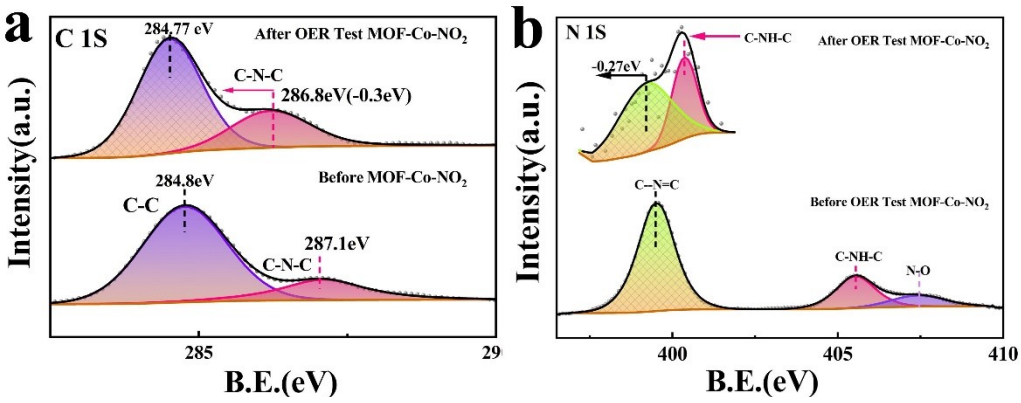

Figure S15. XPS images of C 1S(a), N 1S(b) region survey spectrum of $Co[C_6H_6N_4]NO_2$ samples after OER test.

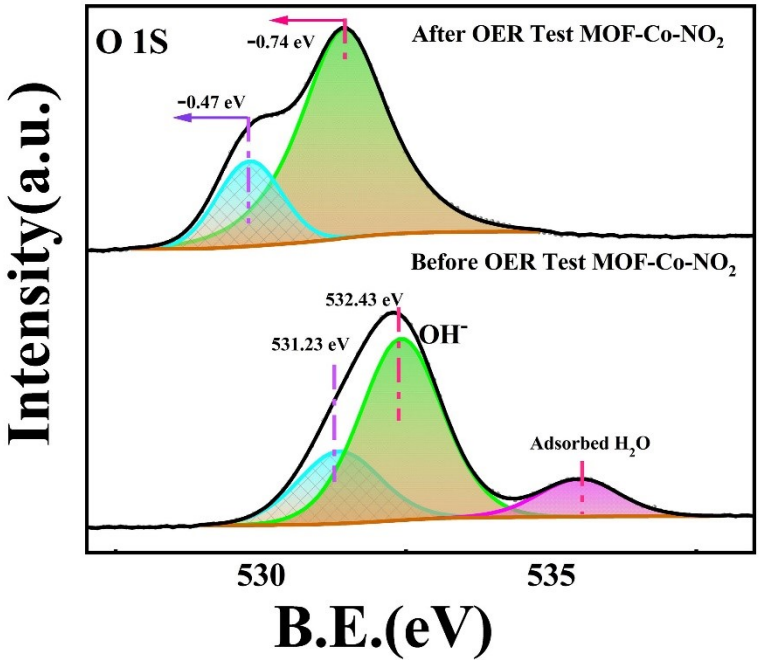

Figure S16. XPS images of O 1S(a) region survey spectrum of $Co[C_6H_6N_4]NO_2$ samples after OER test.

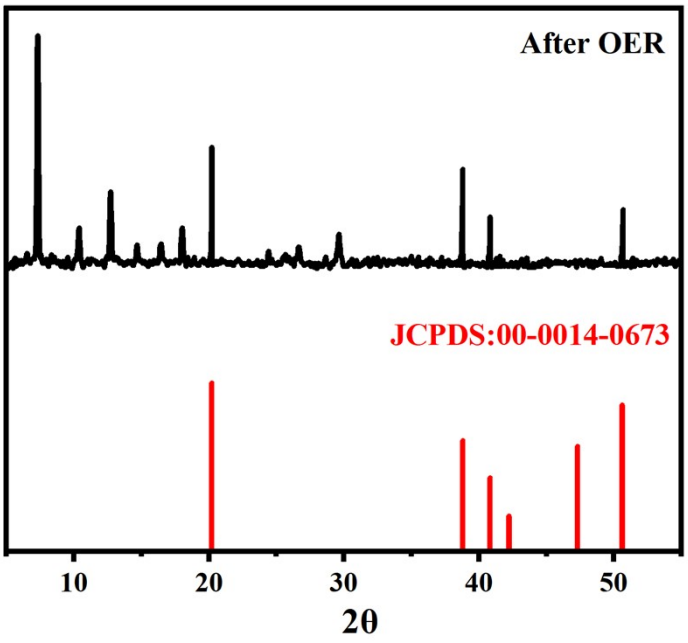

Figure S17. XRD pattern of $Co[C_6H_6N_4]NO_2$ after OER reaction.

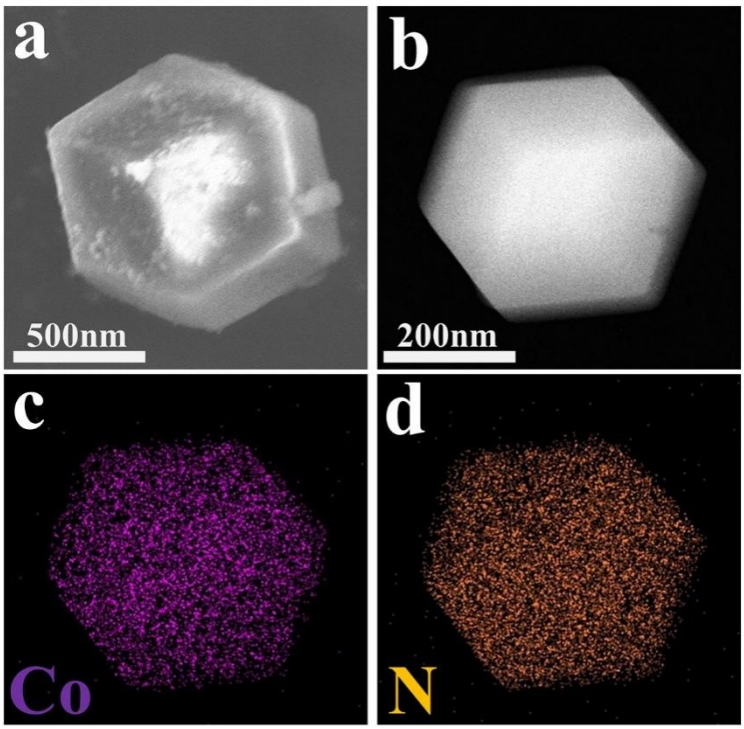

Figure S18. (a) SEM images, (b) TEM image and (c, d) EDX images of the sample $Co[C_6H_6N_4]NO_2$ after OER test.